WESTERN REGION TECHNICAL ATTACHMENT
NO. 88-15
April 12, 1988

REVIEW OF THE NMC NUMERICAL GUIDANCE SUITE IN 1987 AND A PREVIEW OF CHANGES IN 1988 PART II

Ronald D. McPherson, Editor
Meteorological Operations Division

3. Changes in the Medium-Range Forecast System: Masao Kanamitsu

Several changes were implemented in the MRFS on August 12, and the combined modified system is referred to as MRF87. The changes are summarized below.

Increased Horizontal Resolution:

In a major move, the truncation of the series representation of the model's history variables was changed from R40 to T80. This change doubles the resolution in the east-west direction--the minimum resolvable wave is now 4.5 degrees of longitude from crest to crest--and increases the north-south resolution by about 20%. The gaussian grid (the grid mesh on which physical processes are calculated) is now 243 points E/W by 122 points N/S, or approximately 160km mesh length; an exception is the radiation parameterization, which is calculated on a coarser grid of 162x81 points.

By being very careful with the numerical techniques and programming procedures, the running time increased from 16 minutes per day to 24 minutes per day, or only a 50% increase instead of the much larger increase normally expected with a doubling of resolution.

An interesting aspect of this change is that the T80 silhouette orography turns out to be generally lower than the R40 orography.

Radiation:

Several changes were introduced in the radiation parameterization, a part of the MRFS vital to successful performance in the medium- and long-ranges. First, a simple diurnal cycle was introduced. Here, the radiative fluxes--which are calculated only every 12 hours for computational economy--are prorated over each 12 hour interval by the cosine of the solar zenith angle, as illustrated in Figure B-2.

Secondly, the computer program was modified to calculate the fluxes in the vertical structure of the NMC forecast model, rather than on the vertical structure of the original program

as received from the Geophysical Fluid Dynamics Laboratory.

Thirdly, a correction was introduced in the cloud parameterization which uses only a zonal average of climatological cloud distribution, to better account for the effects of cirrus clouds in the tropics.

Fourthly, corrections were introduced for the effects of water vapor and carbon dioxide on long wave radiation.

Finally, the computer program was partially vectorized for more efficient computation on the Cyber 205.

The result of these changes is a more realistic representation of radiative effects on the atmosphere, especially the inclusion of a diurnal cycle. An illustration of this is included as Figure B-3, showing the diurnal variation of skin temperature at a point in the Sahara desert.

Cumulus Parameterization:

The principal change in representing the effects of deep convection was to adapt the NGM procedure, which is similar to the previous MRFS scheme (also based on work by Kuo) but which is fully vectorized and thus much more efficient. It also is one more step in unifying the physics packages of the two systems.

With the introduction of the NGM procedure, it was decided to eliminate the dry convective adjustment as it is no longer needed. This has been present in all NMC models since the mid 1960's as insurance against instability. Also eliminated was the artificial inflation of the parcel temperature by 1^{o}. In another relatively minor change, the calculation of the integral of the moisture tendency was corrected to be the depth of the cloud instead of from the ground to the cloud top. The latter two changes are likely to have only subtle effects on the forecasts.

Figure B-4 illustrates some of the effects of these changes. It contains two zonal mean cross-sections, one for height, and one for specific humidity. The differences in the MRF86 and MRF87 6 h forecasts in the GDAS are shown, averaged over 22 cases in June 1987. The most impressive changes are in the tropical moisture, where the lowest levels are more moist, and the middle troposphere dryer. Thus, in the new MRFS, a known error in the moisture analysis and forecast has been reduced.

Time Scheme:

Changes were introduced in the time-marching scheme for the surface temperature equations, in the calculation of vertical diffusion, and in the calculation of sensible and latent heat fluxes. Figures B-5 and 6 give the details for the numerically curious. Figure B-7 shows a dramatic example of

the effect. In the upper part of the diagram, the skin temperature at a point over the Amazon Basin exhibits time-step-scale oscillations during the time of maximum temperature. This is almost completely eliminated with the corrections.

The aggregate effect of such changes on model output seen by forecasters is probably subtle, and understood only by long-term studies of model characteristics.

Gravity-Wave Drag:

A common systematic error among medium-range numerical models is a tendency toward more zonal flow with time into the forecast period. Nearly all such models tend to lose amplitude of wave features and increase the zonal wind. It has been postulated that the effects of gravity-wave drag, not accounted for in most models until recently, could be responsible for this error. In the atmosphere, flow over major mountain barriers generates gravity waves which propagate vertically as well as horizontally. The vertical propagation results in the transfer of momentum from low-windspeed regions near the earth's surface to high wind regions near the tropopause, where the waves tend to break and dissipate. The practical effect of this is to slow down the winds near the tropopause; hence the term "drag".

Figure B-8 outlines the gravity wave drag parameterization introduced into MRF87. Its effects can be seen in Figure B-9, from an experimental 30-day run of MRF87 from January 4, 1987 initial data. Note that the effect of gravity wave drag is to reduce the error over most of the northern hemisphere (where most of the mountains are), with maximum reduction of 5m/s in the mid-latitude jet region. Little impact is seen in the southern hemisphere.

Most of the impact of the gravity wave drag parameterization will be noted in the longer periods of the forecast; i.e., beyond five days.

Physical Processes

(1) Radiation (called every 12 hours)

- Longwave — Fels and Schwarzkopf (1975)
- Shortwave — Lacis and Hansen (1974)

⊙ Diurnal variation

- Approximation (Campana, 1986)

$$F_{sw} = \begin{cases} \dfrac{\mu(t)}{\bar{\mu}} \bar{F}_{sw} & ; \ \mu(t) > 0 \\ 0 & ; \ \mu \leqq 0 \end{cases}$$

$$\bar{F}_{sw} = \bar{\mu} S T_{ro} \qquad \text{where} \quad \bar{(\ )} = \frac{\int_{daylight} (\ )\, dt}{\int_{daylight} dt}$$

μ : cos (solar zenith angle)

S : solar constant

T_{ro} : atmospheric transmissivity

FIGURE B-2

Sahara

Soil surface temperature

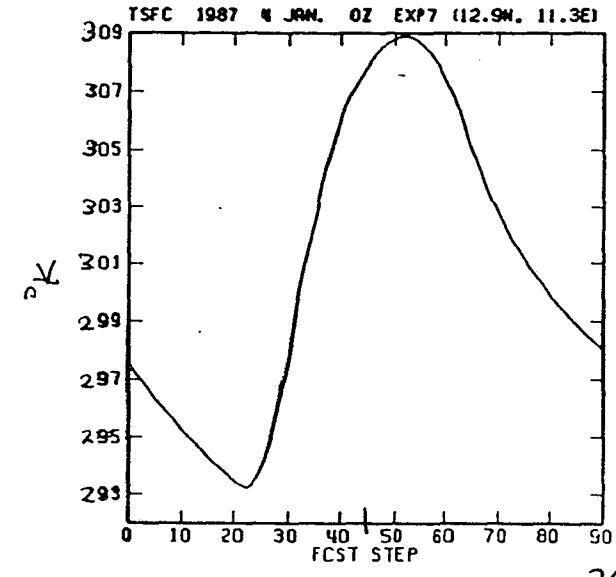

FIGURE B-3

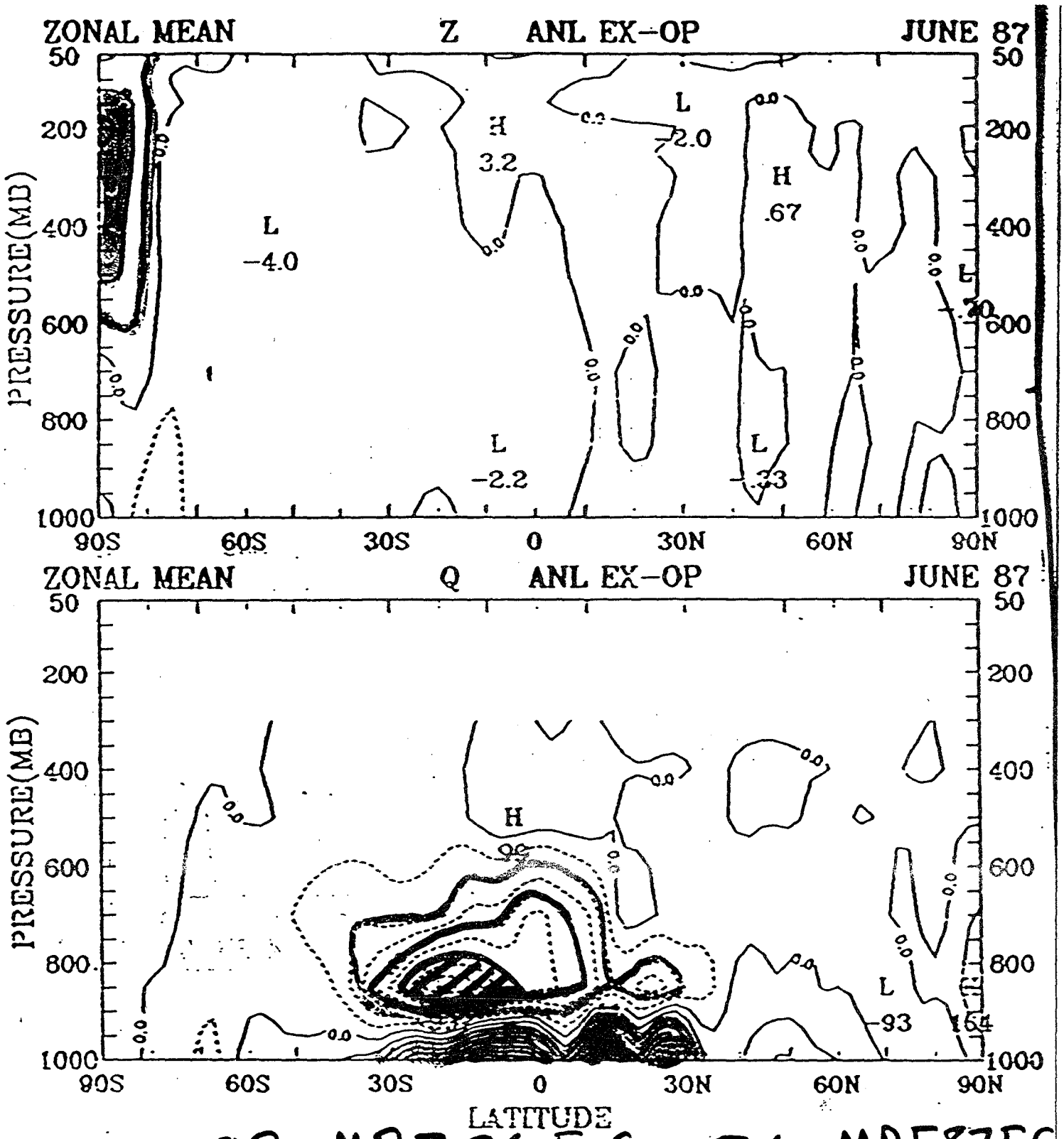

Fig. 8.1. Latitude-pressure cross-sections of the zonal mean differences between the operational R40 and the new T80 analyses of (top) geopotential height and (bottom) specific humidity, averaged over 22 analyses in June 1987. Contour interval 5 m (top), 0.1 g/kg (bottom).

4. Time Scheme (Kalnay, Kanamitsu)

Highly Non-Linear Damping eq.

- Surface Temperature eq.

$$X^* = X^n + k^n X^* \Delta t$$

$$X^{n+1} = (X^n + X^*)/2$$

- Vertical diffusion

$$X^* = X^{n-1} + k^{n-1} X^* \cdot (2\Delta t)$$

$$X^{n+1} = (X^{n-1} + X^*)/2$$

FIGURE B-5

5. Correction to Surface Fluxes

(Silva Dias, Kanamitsu)

- Sensible heat flux

Surface Process	Vertical Diffusion
$\propto (T_g^{n+1} - T_1^n)$	$\propto (T_g^{n+1} - T_1^{n+1})$

results in 10 ~ 20 watts/m² difference

- Latent heat flux

Surface Process	Vertical Diffusion
$\propto \left\{ q_{sg}^n + \frac{\partial q_s}{\partial T}(T_g^n - T_g^{n+1}) - q_1^n \right\}$	$\propto (q_{sg}^{n+1} - q_1^{n+1})$

results in 20 ~ 30 watts/m² difference

FIGURE B-6

old

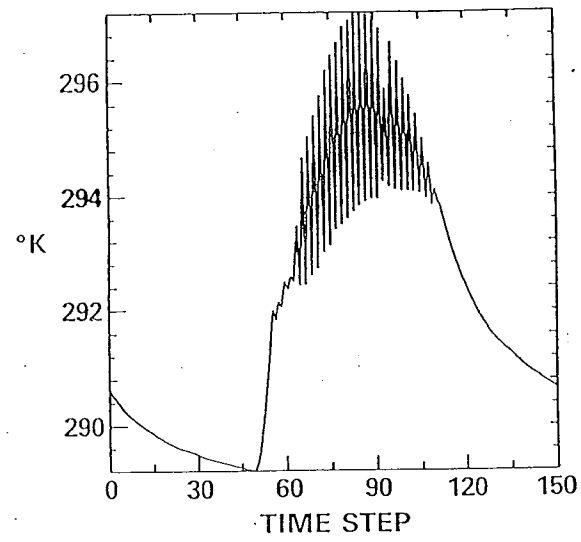

new

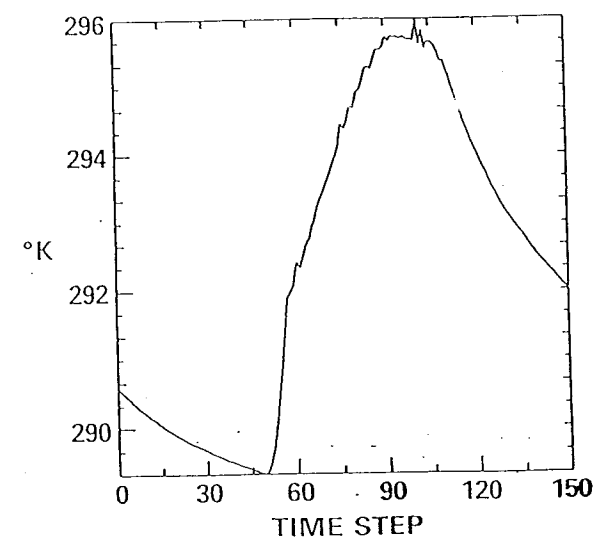

FIGURE B-7 Effect of time filter on a point over Amazons.

6. Gravity Wave Drag

(Alpert, Kanamitsu, Kalnay)

- Surface Stress — Pierrehumbert (1986)

$$\tau_B = -\frac{\rho U^3}{N l^*} G(F_R)$$

$$G(F_R) = \hat{G}\,\frac{F_R^2}{F_R^2 + d^2}$$

$$F_R = \frac{Nh'}{U} \quad , \quad N = -\frac{g^2 \sigma}{\theta R T}\,\frac{\partial \theta}{\partial \sigma}$$

- Vertical Deposition — Helfand et al (1987), Palmer et al (1986)

$$\text{Critical } Fr = 1 - \frac{1}{4Ri}$$

$$\text{local } Fr = \sqrt{\frac{N^2 \tau_{k-1}}{k \rho U^3}}$$

FIGURE B-8

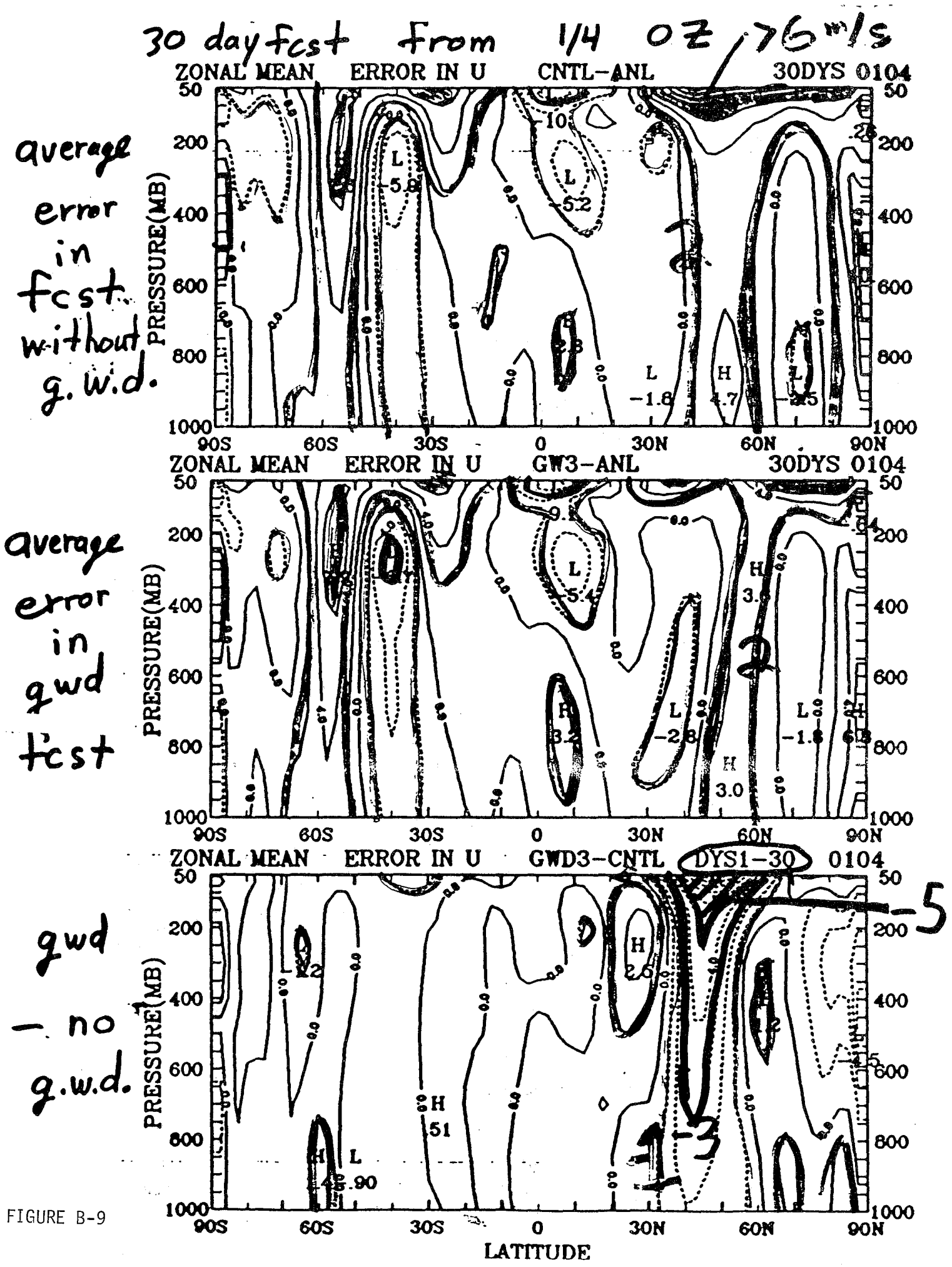
30 day fcst from 1/4 0Z / 76 m/s
average error in fcst without g.w.d.
ZONAL MEAN ERROR IN U CNTL-ANL 30DYS 0104
average error in gwd fcst
ZONAL MEAN ERROR IN U GW3-ANL 30DYS 0104
gwd - no g.w.d.
ZONAL MEAN ERROR IN U GWD3-CNTL DYS1-30 0104
PRESSURE(MB)
50
200
400
600
800
1000
90S
60S
30S
0
30N
60N
90N
LATITUDE

FIGURE B-9